Evidence for eight node mixed-symmetry superconductivity in a correlated organic metal: Supplemental Information

Daniel Guterding,[1] Sandra Diehl,[2,3] Michaela Altmeyer,[1] Torsten Methfessel,[3] Ulrich Tutsch,[4] Harald Schubert,[4] Michael Lang,[4] Jens Müller,[4] Michael Huth,[4] Harald O. Jeschke,[1] Roser Valentí,[1] Martin Jourdan,[3] and Hans-Joachim Elmers[3,*]

[1] *Institut für Theoretische Physik, Goethe-Universität Frankfurt, Max-von-Laue-Str. 1, 60438 Frankfurt am Main, Germany*
[2] *Graduate School Materials Science in Mainz, Staudingerweg 9, 55128 Mainz, Germany*
[3] *Institut für Physik, Johannes Gutenberg-Universität Mainz, Staudingerweg 7, 55128 Mainz, Germany*
[4] *Physikalisches Institut, Goethe-Universität Frankfurt, Max-von-Laue-Str. 1, 60438 Frankfurt am Main, Germany*

(Dated: April 20, 2016)

I. EXPERIMENTAL CRYSTAL ORIENTATION

The height profile measured across the insulating and conducting layers shown in the STM image (Fig. 1 in the main text) carries mostly topographical information. The insulating anion-layers are expected to appear slightly lower (darker) than the conducting BEDT-TTF layers, which is indeed observed but it is, however, a small contribution. Therefore, one can deduce the tilting angle from a comparison to the known crystal structure. By analyzing the height profile along a single unit cell we determine the orientation of the cutting plane (see Fig. 1). Depending on the rotation about the c-axis (the axis perpendicular to the conducting layers) the height corrugation caused by the alternating orientation of the BEDT-TTF molecules is more or less pronounced. The best agreement between height profile and crystal structure is found for a tilting angle $\varphi_{ab} = 60^\circ$ about the c-axis with respect to the b-axis.

II. EXPERIMENTAL EXTRACTION OF THE SUPERCONDUCTING DOS

In STS, the spectra have to be corrected for the different work functions of tip and sample which leads to a voltage-dependent asymmetric tunneling transmission function $T(V)$[1]. For this reason all spectra shown here are normalized to $T(V)$ which was obtained from spectra taken at 13 K, *i.e.*, in the normal state of κ-Br. We furthermore assume a constant DOS for the tip material in the relevant energy range so that the $dI/dV/T(V)$ curves reflect the thermally smeared DOS $D(V)$ of the sample with $eV = E - E_\mathrm{F}$ (E_F denotes the Fermi energy). Then we analyze this data in the framework of the Anderson-Hubbard (AH) model discussed by Shinaoka and Imada[2] for disordered itinerant electron systems with short-range interactions[3].

In their numerical treatment of the AH model a scaling law is introduced for the DOS in the presence of short-range Coulomb interactions and a multi-valley energy landscape[2]: $B(V) = c\exp[-\alpha\,(-\log|eV|)^d]$, $|V| \geq V_0$, where d denotes the spatial dimension ($d = 2$ for the present case) and $\alpha = 0.288$ is a non-universal constant. In the immediate vicinity of E_F the AH model is not applicable[2]. A very good description of this energy region is obtained by assuming a hard energy gap of small size accounted for by a phenomenological DOS function of the following form: $B(V) = c'\cosh(\frac{eV}{\varepsilon_T})$, $|V| < V_0$, where c' is a constant and ε_T measures the effective barrier height. For finite temperatures $T > 0$, $B(V)$ rapidly becomes non-zero near E_F because a thermally activated crossing of the small barrier ε_T leads to a nearly temperature-independent prefactor and the voltage-dependence is described by the cosh term. With the requirement of continuous differentiability at the inflection point V_0, c' and ε_T terms are fixed for any given temperature and do not represent adjustable parameters. The conductance spectrum of the superconducting state is given by

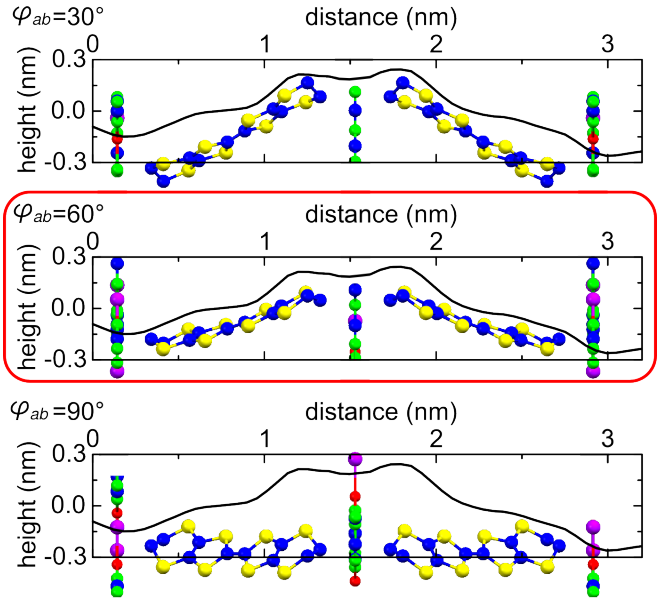

FIG. 1. Height profile along a single unit cell with the corresponding crystal orientation showing the best agreement for an angle for rotation about the c-axis of $\varphi_{ab} = 60^\circ$.

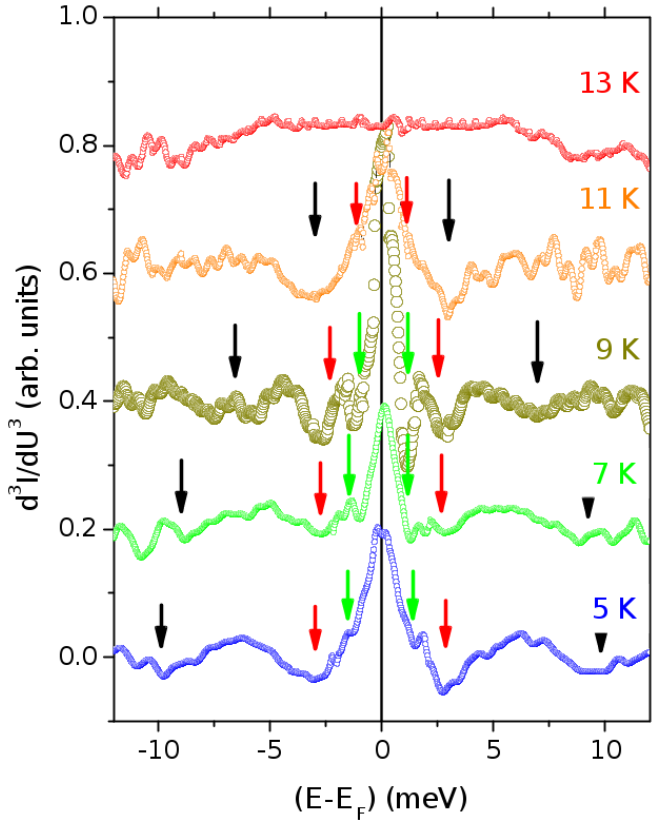

FIG. 2. Temperature dependence of the second derivative of the conductance spectrum $\mathrm{d}I/\mathrm{d}V/T(V)$. Features A, B and C are indicated by the colored arrows (black, red and green respectively).

$S(V) = dI/dV/T(V)/B(V)$.

III. TEMPERATURE DEPENDENCE OF FEATURES OBSERVED IN THE RAW CONDUCTANCE

In Fig. 3 of the main paper we have shown the second derivative of the conductance spectrum $\mathrm{d}I/\mathrm{d}V/T(V)$ at $T = 5$ K. For completeness, the temperature dependence of this quantity is shown in Fig. 2. The temperature evolution of the superconducting gaps associated with features A, B and C can be traced clearly. All gaps decrease when increasing the temperature towards T_c. In the spectrum taken at $T = 13$ K $> T_c$ all signatures of a superconducting gap are gone.

The second derivative of the tunneling conductance was calculated after smoothing the data using the Savitzky-Golay method[4], which is a widely used technique to increase the signal-to-noise ratio without significantly distorting the signal data. The averaging interval is 2.3 meV in the interval [-2.09:2.09] meV and 6 meV outside of this interval. Different smoothing intervals are justified because the noise increases with increasing absolute tunneling current. Thus the noise is considerably lower in the close vicinity of $E - E_F = 0$.

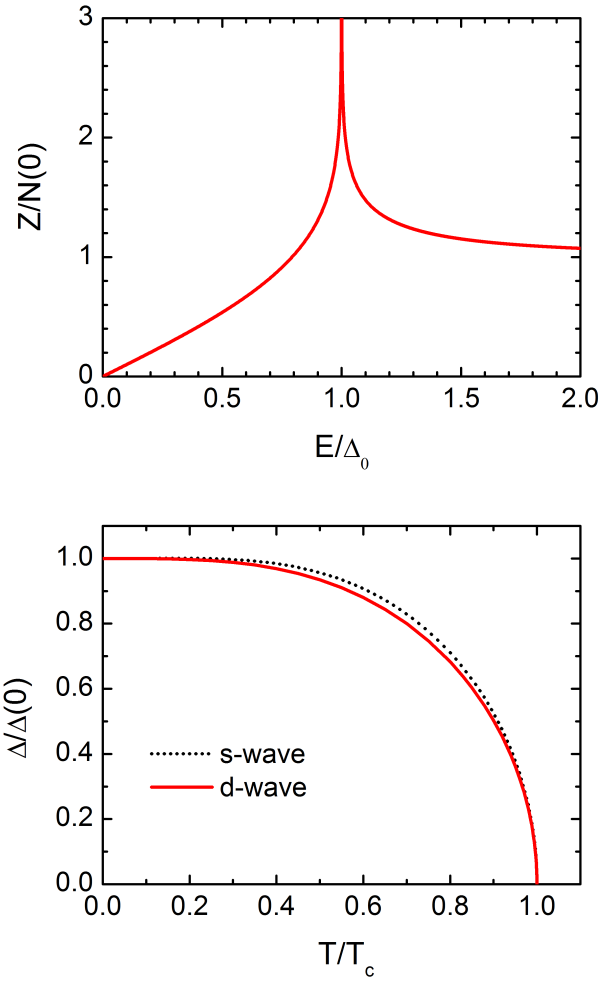

FIG. 3. Density of quasiparticle excitations and energy gap. The upper graph shows the density of quasiparticle excitations in the superconduting state (weak-coupling d-wave) normalized to the density of states at the Fermi edge in the normal-conducting state as function of the excitation energy normalized to the maximum value of the energy gap. In the lower graph the normalized energy gap as function of temperature (normalized to T_c) is shown for the weak-coupling d-wave (red curve) and s-wave (black dotted curve) case.

IV. ANALYSIS OF SPECIFIC HEAT MEASUREMENTS

A method for calculating the specific heat of an unconventional superconductor from first principles has not been developed yet. Therefore, we have performed calculations of the specific heat of κ-Br in the framework of the multi-band alpha model for d-wave superconductors in order to check for compatibility of the gap parameters, as derived from our STS data, with specific

heat results from the literature[5]. The alpha model for s-wave superconductors, introduced by Padamsee et al.[6], extends BCS theory in a purely phenomenological way to materials with arbitrary (positive) values of the ratio $\alpha = \Delta(0)/k_{\mathrm{B}}T_c$. As low temperature specific heat data for κ-Br indicate nodes in the gap function[5] (d-wave) as do our STS results (extended $s + d_{x^2-y^2}$), we extend the alpha model to the d-wave case. This can be done once the density of quasiparticle excitations $Z_d(E)$ and the gap function $\Delta_d(k,T)$ are known for this case. These two quantities have been calculated using BCS theory with a cylindrical Fermi surface and a gap function of the type $\Delta_d = \Delta_0(T)\cos(2\varphi)$. As the electronic system of κ-Br shows a strongly two-dimensional character, these approximations can be considered as an appropriate simplification for estimating the specific heat. The results for $Z_d(E)$ and $\Delta_0(T)$ are shown in Fig. 3. A value of $\alpha = 2.14$ has been obtained for the weak coupling limit consistent with the results of Ref. 7.

The multi-band alpha model, where each of the gaps occurs in a different band, deviates from the one-band scenario (described in the subsequent theoretical parts) which is used for fitting the STS data. However, as the specific heat depends essentially only on the quasiparticle density of states $Z(E)$, we attempt to fit this quantity (known from the theoretical considerations and the fitting of the STS data) by a sum of d-wave quasiparticle densities of states, each with its own maximum gap value $\Delta_{0,i}(T)$, i.e., with a multi-band alpha model. As an approximation to the density of states derived by the microscopic theory (blue line in Fig. 4) we use the function

$$[Z(E)/N(0)]_{\mathrm{fit}} = \sum_{i=1}^{n} g_i \, z_d(E/\Delta_{0,i}(T)) \qquad (1)$$

with $z_d(E/\Delta_{0,i}(T))$ and $\Delta_{0,i}(T)/\Delta_{0,i}(0)$ being the d-wave functions shown in Fig. 3, $N(0)$ the density of states at the Fermi edge in the normal-conducting state and $\sum_{i=1}^{n} g_i = 1$. Here g_i and $\Delta_{0,i}(0)$ are used as adjustable parameters. In our case three bands are needed, as the quasiparticle density of states shows three local maxima (see Fig. 4). The so-derived fitting function $[Z(E)/N(0)]_{\mathrm{fit}}$ with the parameter values $g_1 = 0.08$, $g_2 = 0.54$, $g_3 = 0.38$ and $\Delta_{0,1}(0) = 0.48\,\mathrm{meV}$, $\Delta_{0,2}(0) = 2.58\,\mathrm{meV}$, $\Delta_{0,3}(0) = 9.20\,\mathrm{meV}$ is displayed in Fig. 4 (red dotted curve) and shows a fairly good agreement with the theoretical results. Using a T_c value of 11.2 K, as obtained from the theoretical fit to the STS derived $\Delta_0(T)$ points, we get $\alpha_1 = 0.50$, $\alpha_2 = 2.67$, $\alpha_1 = 9.53$. The specific heat of the three-band alpha model is then given by

$$C = \sum_{i=1}^{3} C_d(T, T_c, \gamma_i, \alpha_i) \qquad (2)$$

with $\gamma_i = g_i\,\gamma$. The result of this calculation for the specific heat is shown in Fig. 5 (blue curve) together with

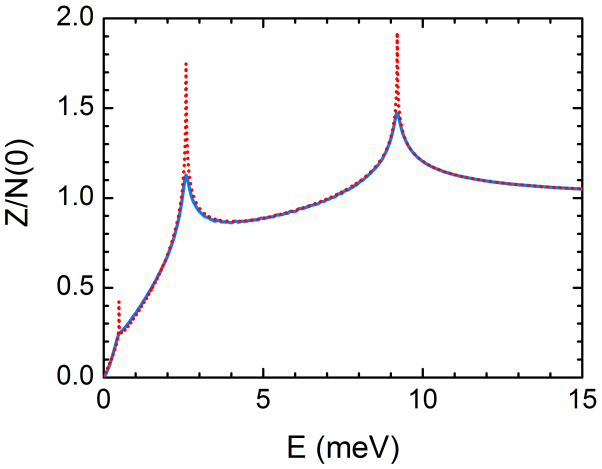

FIG. 4. Density of quasiparticle excitations for κ-Br. Normalized quasiparticle density of states for the parameter values (at $T = 5$ K) given in Table I of the main text with a small broadening of $\Gamma = 0.07\,\mathrm{meV}$ (blue curve) and for the three-band alpha model (red dotted curve) with $g_1 = 0.08$, $g_2 = 0.54$, $g_3 = 0.38$ and $\Delta_{0,1}(0) = 0.48\,\mathrm{meV}$, $\Delta_{0,2}(0) = 2.58\,\mathrm{meV}$, $\Delta_{0,3}(0) = 9.20\,\mathrm{meV}$.

the literature data from Ref. 5. The γ value was set to $27.5\,\mathrm{mJ/(mol\,K^2)}$ as determined by Ref. 5 and a Gaussian T_c distribution ($\sigma = 0.98\,\mathrm{K}$, $\overline{T}_c = 12.0\,\mathrm{K}$) has been used to take into account the rounded maximum of the experimental data. The calculated results are in fairly good agreement with the experimental data. A better (and nearly perfect) fit can be obtained (red curve) by changing the g_i values to $g_1 = 0.04$, $g_2 = 0.76$, $g_3 = 0.20$ and setting $\alpha_2 = 3.10$ (accounting for the dominant contribution to the specific heat), $\sigma = 0.83\,\mathrm{K}$, $\overline{T}_c = 12.1\,\mathrm{K}$.

V. THEORY: BCS DENSITY OF STATES

The basic idea of BCS theory is the Cooper problem, which states that an attractive interaction between two electrons with opposite spin and momentum leads to a bound state, no matter how small it is. The corresponding Hamiltonian for Cooper pairs having a net momentum of zero can be written as

$$H = \sum_{k,\sigma} \epsilon_{k\sigma} c^{\dagger}_{k\sigma} c_{k\sigma} + \sum_{k,k'} U(k,k') c^{\dagger}_{k\uparrow} c^{\dagger}_{-k\downarrow} c_{-k'\downarrow} c_{k'\uparrow}.$$

The interaction can be treated in mean field theory ($\delta(c^{\dagger}c^{\dagger}) = c^{\dagger}c^{\dagger} - \langle c^{\dagger}c^{\dagger}\rangle$), where terms quadratic in δ are neglected. The resulting Hamiltonian can be diagonalized using the Bogoliubov-Valatin transformation, which introduces quasiparticle creation and annihilation operators $\gamma^{\dagger}_{k\sigma}$ and $\gamma_{k\sigma}$. The quasiparticle excitation energies are given as $E_k = \sqrt{\epsilon_k^2 + |\Delta_k|^2}$, where $\Delta(k) = \sum_{k'} U(k,k')\langle c_{-k'\downarrow} c_{k'\uparrow}\rangle$.

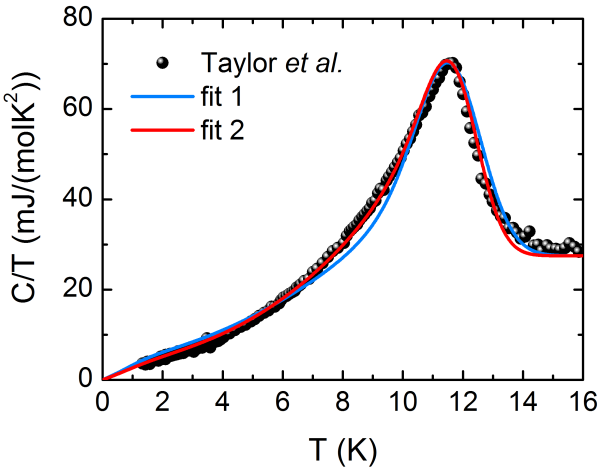

FIG. 5. Specific heat (devided by temperature). Black spheres are data from Taylor et al.[5], blue and red lines indicate our fits with the three-band alpha model for d-wave superconductors and a gaussian T_c distribution. The parameters of fit 1 (fit 2) are: $\gamma = 27.5\,\mathrm{mJ/(mol\,K^2)}$, $g_1 = 0.08\,(0.04)$, $g_2 = 0.54\,(0.76)$, $g_3 = 0.38\,(0.20)$, $\alpha_1 = 0.50$, $\alpha_2 = 2.67\,(3.10)$, $\alpha_3 = 9.65$ and $T_c = 12.0\,\mathrm{K}$ (12.1 K), $\sigma = 0.98\,\mathrm{K}$ (0.83 K).

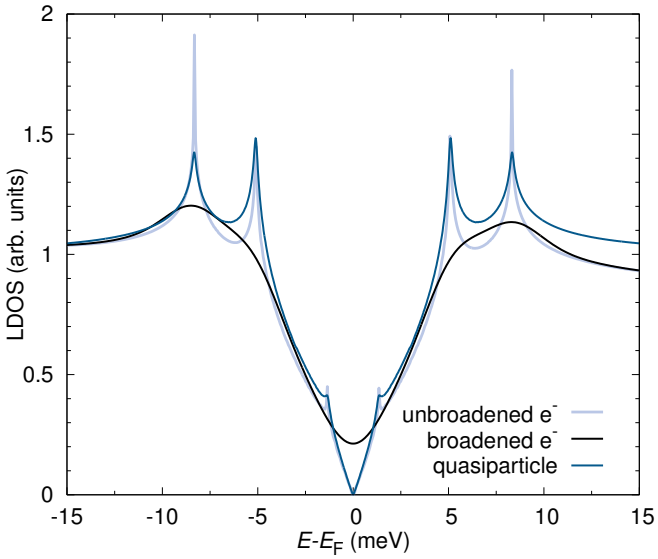

FIG. 6. Comparison of broadened and unbroadened electron DOS to the quasiparticle DOS for identical parameters (as given in Table I). The quasiparticle DOS includes a small broadening of $\Gamma = 0.07$ meV. The energy scale is set to $\Delta_0 = 10$ meV.

The BCS Hamiltonian in terms of the quasiparticle creation and annihilation operators reads

$$H_{\mathrm{BCS}} = \sum_{k,\sigma} E_k \gamma^\dagger_{k\sigma}\gamma_{k\sigma} + \sum_k \epsilon_k - \sum_{k,k'} U(k,k')\langle c^\dagger_{k\uparrow} c^\dagger_{-k\downarrow}\rangle\langle c_{-k'\downarrow} c_{k'\uparrow}\rangle.$$

The excitation spectrum of the quasiparticles E_k is gapped and defined only for positive energies. The density of states of quasiparticles in an isotropic s-wave superconductor ($\Delta_k = \Delta_0$) can be calculated via

$$\begin{aligned}\rho_{\mathrm{qp}}(E) &= \frac{1}{N}\sum_k \delta(E - E_k) \\ &= \int d\epsilon \rho_0(\epsilon) \frac{\sqrt{\epsilon^2 + |\Delta|^2}}{\epsilon} \delta(\epsilon - \sqrt{E^2 - |\Delta|^2}) \\ &= \begin{cases} \rho_0(\sqrt{E^2 - |\Delta|^2}) \frac{E}{\sqrt{E^2 - |\Delta|^2}} & E > |\Delta| \\ 0 & E < |\Delta| \end{cases}.\end{aligned}$$

As the quasiparticles are superpositions of particles and holes, this is not the density of states that can be measured in, for instance, scanning tunneling spectroscopy. To determine the electron DOS, we have to start from another commonly used expression of the density of states in terms of Greens functions, $\rho(E) = -\frac{1}{\pi}\sum_{k\sigma} \mathrm{Im}(-\langle c^\dagger_{k\sigma} c_{k\sigma}\rangle_0)$.

We assume a non spin-polarized energy dispersion and again insert the Bogoliubov-Valatin transformation

$$\rho(E) = \frac{2}{\pi}\sum_k \mathrm{Im}\left(|u_k|^2 \left\langle \gamma^\dagger_{k\uparrow}\gamma_{k\uparrow}\right\rangle_0 + |v_k|^2 \left\langle \gamma_{-k\downarrow}\gamma^\dagger_{-k\downarrow}\right\rangle_0\right).$$

As the Hamiltonian is diagonal in the quasiparticle operators, we can insert the expression for the bare Greens function and get

$$\rho(E) = 2\sum_k \left(|u_k|^2\delta(E - E_k) + |v_k|^2\delta(E + E_k)\right),$$

where k is a combined momentum and band index. $|u_k|^2$ and $|v_k|^2$ are the probabilities for the excitations being hole- or electron-like respectively. Only positive energies are taken into account[8].

Next we calculate the DOS explicitly for the *ab initio* derived bandstructure and the superconducting gap calculated microscopically. The delta functions in the DOS are replaced by gaussians with a standard deviation of 1.2 meV to simulate the broadening observed in experiment. For comparison we also calculated the DOS with a tetrahedron method[9] that does not employ any broadening. For the calculation of the DOS using gaussians we included 4000×4000 k-points in the xy-plane. In the tetrahedron method we used $4000 \times 4000 \times 2$ k-points.

A comparison of the broadened and unbroadened electron DOS and the quasiparticle DOS is shown in Fig. 6. Peak positions are identical. Only the background far away from the Fermi level is not well represented by the quasiparticle approximation. This can be easily understood from the structure of the expression derived before. To one energy E two different electron energies ϵ_k and

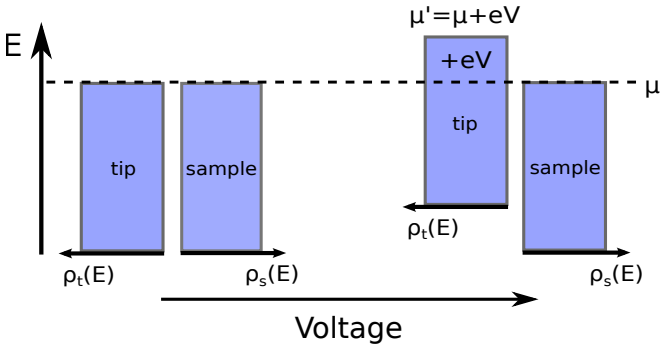

FIG. 7. Illustration of the energy levels in tip and sample with (right) and without (left) applied voltage. The voltage raises the energy levels of the tip, so that the chemical potential is higher than in the sample and a net current results. Note, that these energy shifts in the tip can be described in two ways: $f(E, \mu' = \mu + eV)$ or $f(E - eV, \mu)$.

$\epsilon_{k'}$ (where $\epsilon_k = -\epsilon_{k'}$) contribute and the BV coefficients should average to approximately $\sqrt{0.5}$. The small deviations are causing the asymmetric behavior, which merges to the normal density of states far away from the gap.

In the case of an anisotropic gap, the normal state density of states can not be identified easily, because the gap Δ then also depends on momentum k and the Fermi surface is not a concentric circle.

$$\rho_s(E) = \int d\epsilon \frac{1}{N} \sum_k \delta(\epsilon - \epsilon_k)\delta(|E| - \sqrt{\epsilon^2 + |\Delta_k|^2}) \neq \int d\epsilon \rho_N(\epsilon)\delta(|E| - \sqrt{\epsilon^2 + |\Delta_k|^2}).$$

However, in the commonly used ansatz the electrons are considered to be free (Fermi surface is a concentric circle) and the gap is only determined by the angle θ

$$\rho_s(E) = \frac{1}{(2\pi)^2} m_e \mathrm{Re} \int d\theta \frac{|E|}{\sqrt{E^2 - |\Delta(\theta)|^2}}.$$

For all further calculations we will use this expression for the quasiparticle DOS.

VI. THEORY: DIFFERENTIAL CONDUCTANCE

In a scanning tunneling spectroscopy (STS) experiment the current *from the tip to the sample* should obey (see Fig. 7),

$$I_{ts}(V) = \frac{2\pi e}{\hbar} \int_{-\infty}^{\infty} dE |M_{ts}(E - eV)|^2 \rho_{\mathrm{tip}}(E - eV) \times f(E - eV)\rho_{\mathrm{sample}}(E)(1 - f(E)),$$

where e is the positive elementary charge and a positive voltage V corresponds to net charge carrier transport into the sample. The current is proportional to the tunneling probability $|M_{ts}(E)|^2$, which depends on tip and sample geometry. Furthermore, the tunneling probability is proportional to the number of occupied states in the tip $\rho_{\mathrm{tip}}(E - eV)f(E - eV)$ and the number of unoccupied states in the sample at lower energies $\rho_{\mathrm{sample}}(E)(1 - f(E))$.

After shifting the integration variable $E \to E + eV$, we arrive at the literature form of the expression for the tunneling current. In order to obtain the net current, we have to calculate the difference between the currents from *tip to sample* and *sample to tip*. We obtain

$$I(V) = \frac{2\pi e}{\hbar} \int_{-\infty}^{\infty} dE |M_{ts}(E)|^2 \rho_{\mathrm{tip}}(E)\rho_{\mathrm{sample}}(E + eV) \times (f(E) - f(E + eV)).$$

The tunneling matrix element $|M_{ts}(E)|^2$ is experimentally not accessible and therefore the tunneling current is divided by the voltage dependent tunneling transmission function $T(V)$, which can be determined from the experimental setup. The density of states of the tip is considered to be independent of energy in the region of interest. We obtain the differential conductance (shifting once again the integration variable $E \to E - eV$) by taking the derivative with respect to the voltage V,

$$\frac{1}{T(V)} \frac{dI(V)}{dV} = \frac{2\pi e}{\hbar} \rho_{\mathrm{tip}}(E_F) \times \int_{-\infty}^{\infty} dE \rho_{\mathrm{sample}}(E) \left(-\frac{df(E + eV)}{dV} \right).$$

VII. THEORY: BROADENING

In the preceding expression we already included thermal broadening via the Fermi function. Additionally we have to take into account the finite quasiparticle lifetime. This can be done (following Dynes *et al.*[10]) by replacing the energies E by $E + i\Gamma$ in the density of states. If we now consider only proportionalities, we can also insert the angle dependent expression for the sample density of states

$$\frac{dI(V)}{dV} \propto T(V) \int_{-\infty}^{\infty} dE \int_0^{2\pi} d\theta \times \mathrm{Re} \frac{|E + i\Gamma|}{\sqrt{(E + i\Gamma)^2 - \Delta(\theta)^2}} \left(-\frac{df(E + eV)}{dV} \right).$$

Note that this formula can not be used to fit data with large finite values of the differential conductance at zero bias voltage, since the superconducting DOS goes to zero for zero bias voltage, independent of the choice of Γ.

Sometimes a slightly different expression is used for the Dynes broadening: $|\mathrm{Re}[(E + i\Gamma)/\sqrt{(E + i\Gamma)^2 - \Delta(\theta)^2}]|$ Although only taking the real part and calculating the absolute value were exchanged here, this formula yields a finite value for the superconducting DOS at zero bias voltage, which is proportional to Γ. Therefore, one can

name	function	coefficient	value
$s\pm$	$\cos k_x + \cos k_y$	c_{s_1}	0.069
$s\pm$	$\cos k_x \cdot \cos k_y$	c_{s_2}	-0.672
$d_{x^2-y^2}$	$\cos k_x - \cos k_y$	c_{d_1}	-0.259
d_{xy}	$\sin k_x \cdot \sin k_y$	c_{d_2}	0.000

TABLE I. Basis functions considered in the fitting process of the microscopic result for the gap function. Given values are the result of the fitting procedure.

use it to fit data for the differential conductance, which include a constant background. Unfortunately, exchanging the order of the real part and absolute value operations is inconsistent with the expression for the BCS density of states. We fix this problem by introducing the shift of the background explicitly.

VIII. THEORY: FITTING GAP SYMMETRIES TO STS DATA

On top of the broadening effects, it was found that the measured density of states is suppressed by the formation of a soft Hubbard gap caused by short-range interactions and disorder[2]. This correction can be taken into account by scaling the density of states by $B(V)$ as described before. Including this correction the differencial conductance reads

$$\frac{1}{B(V)T(V)}\frac{dI(V)}{dV} \propto \int_{-\infty}^{\infty} dE \int_0^{2\pi} d\theta \times \mathrm{Re}\frac{|E+i\Gamma|}{\sqrt{(E+i\Gamma)^2-\Delta(\theta)^2}} \times \left(-\frac{df(E+eV)}{dV}\right).$$

For anisotropic gaps on Fermi surfaces, which are not concentric circles, this equation is still an approximation. To improve our calculations, we execute the integration over the angle as a summation over points on the discretized two-dimensional *ab initio* Fermi surface. We find from our microscopic calculations that the symmetry of the superconducting gap can be described by a superposition of two $s\pm$ and the $d_{x^2-y^2}$ functions, $\Delta(k_x,k_y) = \Delta_0[(c_{s_1}(\cos(k_x)+\cos(k_y)) + c_{s_2}\cos(k_x)\cos(k_y) + c_{d_1}(\cos(k_x)-\cos(k_y))]$, where the normalized prefactors c_i ($\sum_i |c_i| = 1$) can be a) fitted to the experiment (see Fig. 8), *or* b) set to the microscopic values (see Fig. 9), so that only one common prefactor Δ_0 is fitted to the magnitude of the gap.

The Dynes broadening Γ is used as a fit parameter. The value for the differential conductance in the measured data after dividing by correction terms $B(V)$ and $T(V)$ is still finite. This finite differential conductance at zero bias voltage is too large to be explained by thermal broadening. Therefore, we introduce a parameter x, which scales and shifts the calculated DOS so that a constant background in the differential conductance is subtracted, while keeping the data points far away from the Fermi level at unity. With this additional correction we obtain the final formula given in the main text.

The gap on the Fermi surface is shown in Fig. 10 for both the microscopic ratios and those obtained from the fit to the STS data. The analytic representation for the microscopic results was determined by fitting a linear combination of symmetry functions given in Table I. The largest deviation of the fit from the microscopic gap per evaluated k-point is 4.55% of the maximum gap value. The average deviation of the fit is 1.25% of the maximum gap value. For a comparison of the microscopic result to its analytic representation see Fig. 10.

While Fig. 10 emphasizes the qualitative agreement between experiment and theory, we include also polar and linear plots (see Fig. 11) of the same data to reveal some quantitative differences. The angle φ in the k_x-k_y plane is measured from the k_x direction. For the RPA curves and the fitted result the energy scale was set to $\Delta_0 = 10$ meV and $\Delta_0 = 12.1$ meV respectively. In this way, the RPA result can be compared directly to the data shown in Fig. 6 or the DOS shown in Fig. 4 of the main paper, while the data obtained by analysing the experiment can be compared to Fig. 3 in the main paper.

While the symmetry of the superconducting gap obtained from theory is identical to the one found by fitting the experiment, the size of the superconducting gap around $\varphi \approx 45°$ is clearly overestimated in our calculation. Quantitative differences are however to be expected, as our RPA approach does not take into account the electronic self-energy and lacks a self-consistency condition. Note that there is currently no state-of-the-art method that can quantitatively predict the momentum-resolved gap structure or superconducting transition temperature of two-dimensional correlated electron systems.

Finally, we investigate whether a nodeless anisotropic s-wave symmetry could be present in the system. We combine a plain s-wave gap with the d-wave expressions given in our manuscript and determine the prefactors for the contributions that lead to optimal agreement with the experimental spectrum measured at 5 K (see Fig. 12). For both the $s+d_{xy}$ and $s+d_{x^2-y^2}$ case we observe that the d-wave component is dominant in the optimal fit to the STS data. This excludes a nodeless anisotropic s-wave symmetry. The agreement of the $s+d_{xy}$ symmetry is considerably worse than for the $s+d_{x^2-y^2}$ symmetry. The $s+d_{x^2-y^2}$ and the $s_\pm+d_{x^2-y^2}$ solution presented in our manuscript describe the data equally well. However, as a plain s-wave component cannot be caused by antiferromagnetic spin-fluctuations alone, we decided to use the physically more meaningful representation in terms of an extended s-wave component.

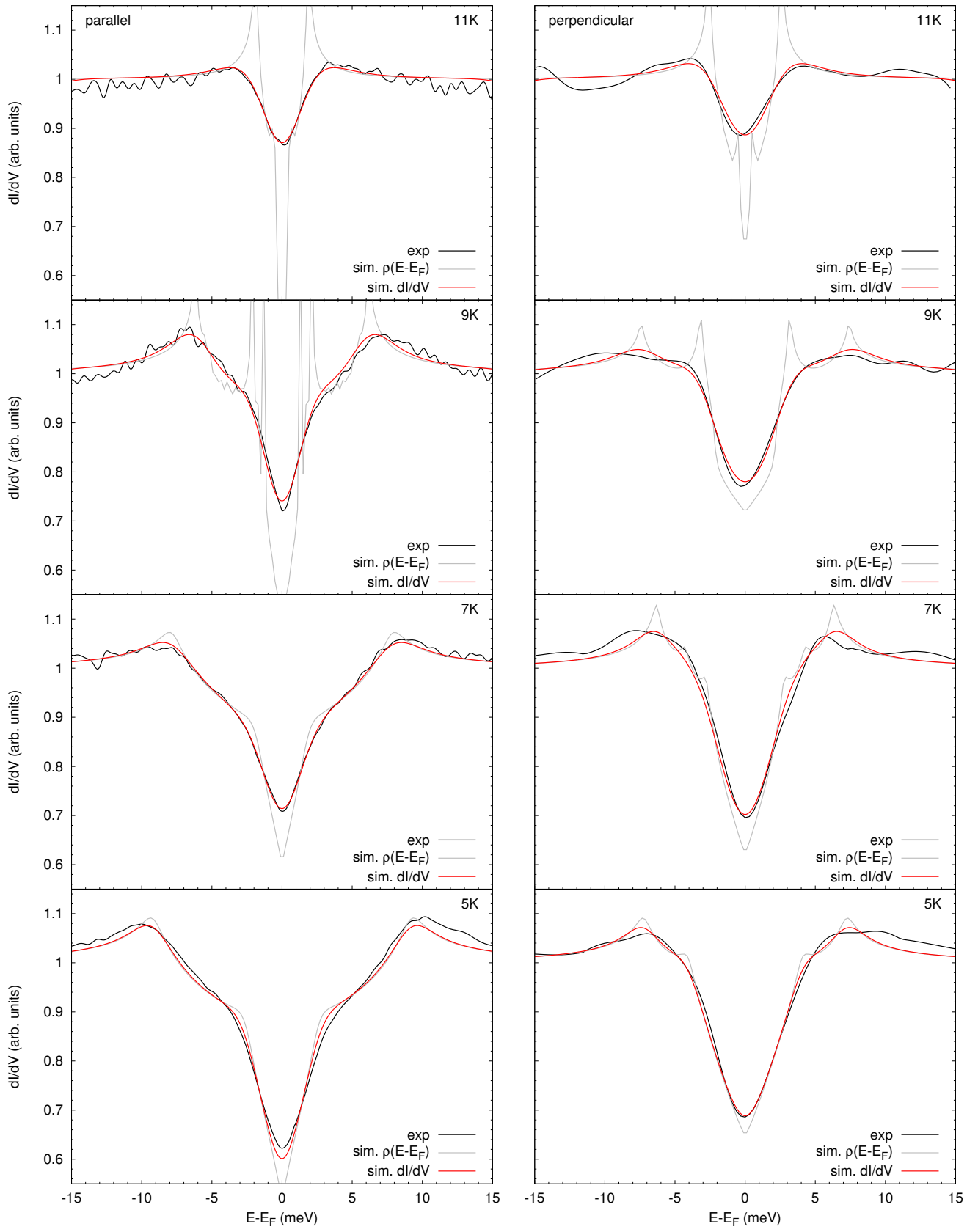

FIG. 8. Fit to the experimental data at the different temperatures (Prefactors are fitted).

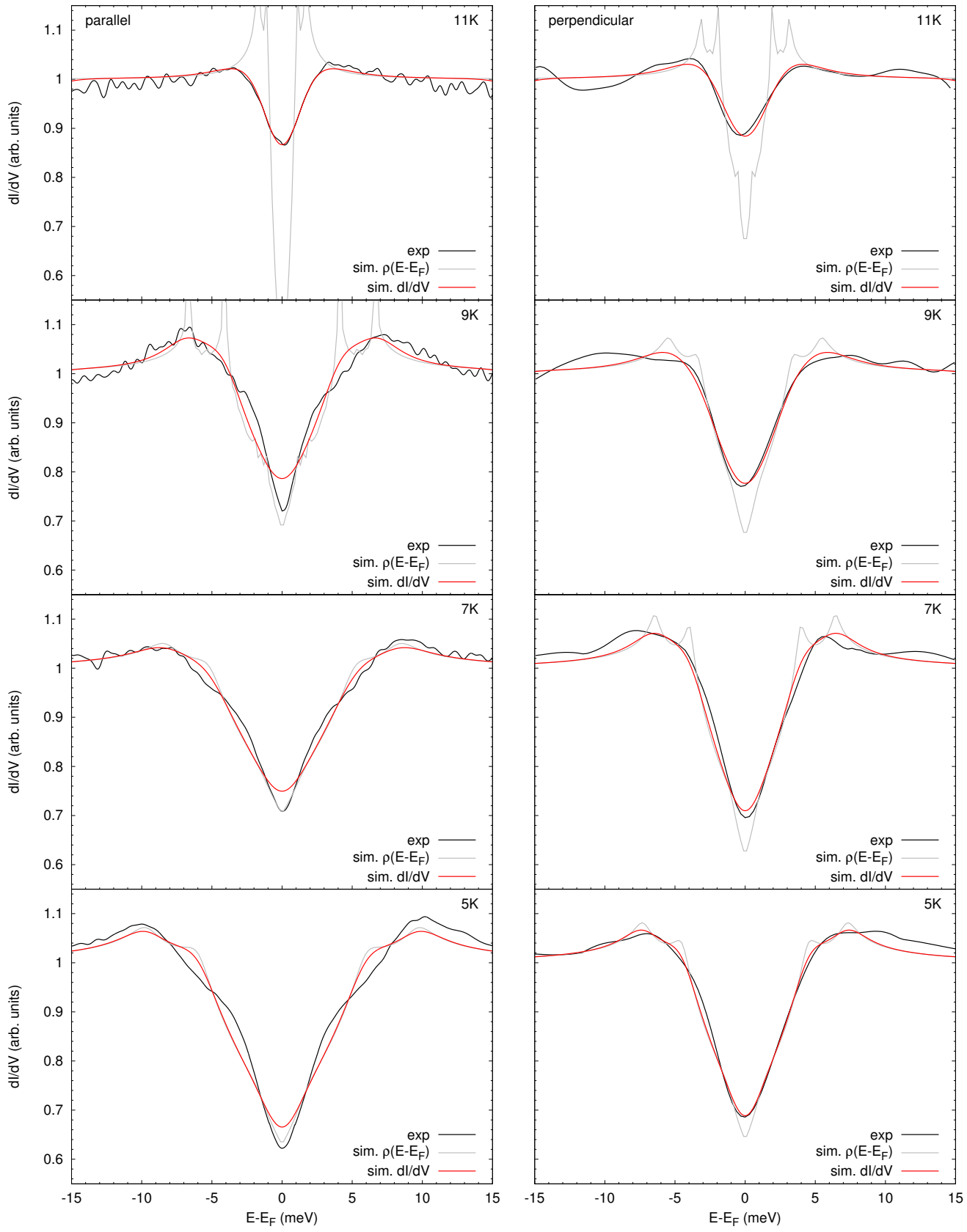

FIG. 9. Fit to the experimental data at the different temperatures (Prefactors fixed to microscopic values).

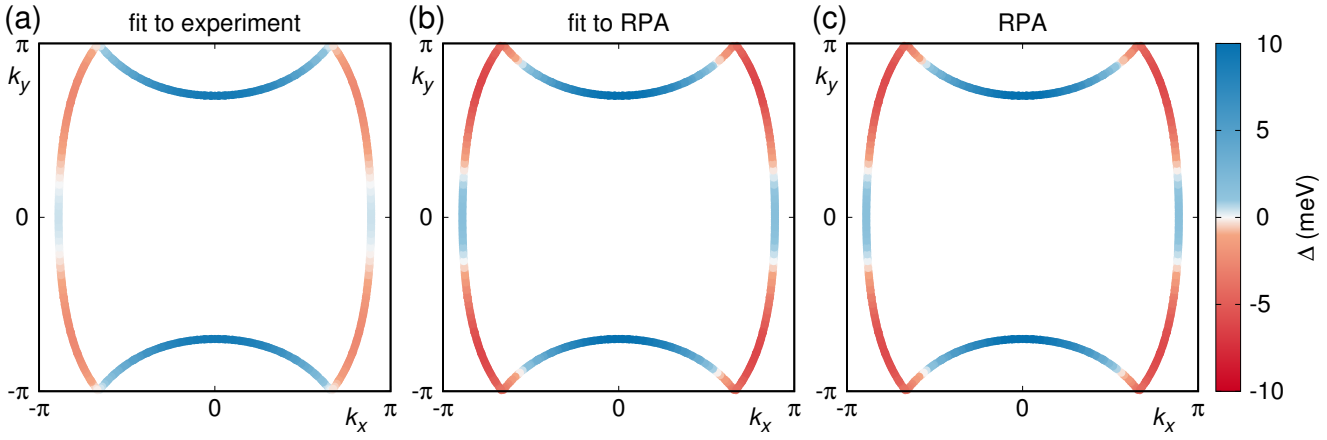

FIG. 10. Comparison of the gap functions on the *ab initio* Fermi surface obtained from (a) fitting the STS experiment (b) fitting the microscopic result calculated using RPA and (c) the microscopic result itself. All data points of the symmetry functions were multiplied by the energy scale $\Delta_0 = 12.1$ eV.

IX. THEORY: TEMPERATURE DEPENDENCE OF THE GAP

To estimate values for the critical temperature and the maximum gap size at zero temperature, we fitted our temperature dependent gap values to the interpolation formula $\Delta(T) = \Delta_0 \tanh(1.74\sqrt{\frac{T_c}{T} - 1})$ for the solution of the s-wave BCS self consistency equation (see Fig. 13).

Solving the BCS self-consistency equation for unconventional pairing mechanisms is difficult due to the momentum dependence of the pairing interaction. Therefore, we decided to use the s-wave solution as a rough approximation.

Our predicted values for the critical temperatures $T_c = 10.3 \pm 1.2$ K for fitted prefactors and $T_c = 11.2 \pm 0.2$ K for fixed prefactors are in good agreement with the experimental observation of $T_c \approx 11.5$ K (see f.i. Ref. 11). The maximal gap size is found to be $\Delta_0 = 12.9 \pm 2.0$ meV (fitted prefactors) and $\Delta_0 = 12.1 \pm 0.7$ meV (fixed prefactors).

X. THEORY: AB-INITIO CALCULATIONS

We use the experimental crystal structure[12], but relax the ethylene endgroups of the BEDT-TTF molecules in eclipsed configuration[13]. For the exchange correlation functional we use the generalized gradient approximation (GGA)[14]. The DFT calculation was converged using $6 \times 6 \times 6$ k-point grids.

XI. THEORY: RPA SPIN-FLUCTUATION PAIRING, FORMALISM

In κ-(BEDT-TTF)$_2$X materials there is strong evidence for antiferromagnetic spin-fluctuations[15]. Therefore, we investigate the superconducting state of these materials based on a random phase approximation (RPA) spin-fluctuation approach[16]. We have generalized our implementation from single-site multi-orbital models[17,18] to multi-site single-orbital models relevant for the materials discussed here.

The low-energy Hamiltonian is given by the kinetic part H_0, derived with the Wannier function method described in the main text, and the intra-orbital Hubbard interaction $H_{\rm int}$.

$$\begin{aligned} H &= H_0 + H_{\rm int} \\ &= \sum_\sigma \sum_{<ij>} t_{ij} c^\dagger_{i\sigma} c_{j\sigma} + \frac{U}{2} \sum_\sigma \sum_i n_{i\sigma} n_{i\bar{\sigma}} \end{aligned}$$

Here, σ represents the spin and $n_{i\sigma} = c^\dagger_{i\sigma} c_{i\sigma}$. The sum over i runs over all BEDT-TTF sites in the unit cell. The hopping integrals t_{ij} taken into account are not restricted to nearest or next-nearest neighbor hoppings. We rather determine the optimal distance cutoff during the wannierization procedure. The interaction strength U is treated as a parameter.

We calculate the non-interacting static susceptibility χ^0, where matrix elements $a^l_\mu(\vec{k})$ resulting from the diagonalization of the initial Hamiltonian H_0 connect orbital and band-space denoted by indices l and μ respectively. The E_μ are the eigenvalues of H_0 and $f(E)$ is the Fermi function.

$$\chi^0_{spqt}(\vec{q}) = -\frac{1}{N_k} \sum_{\vec{k},\mu,\nu} a^s_\mu(\vec{k}) a^{p*}_\mu(\vec{k}) a^q_\nu(\vec{k}+\vec{q}) a^{t*}_\nu(\vec{k}+\vec{q}) \times \frac{f(E_\nu(\vec{k}+\vec{q})) - f(E_\mu(\vec{k}))}{E_\nu(\vec{k}+\vec{q}) - E_\mu(\vec{k})}$$

In our calculation both $\vec{q}$ and $\vec{k}$ run over uniform grids spanning the reciprocal unit cell. Temperature enters the calculation through the Fermi functions.

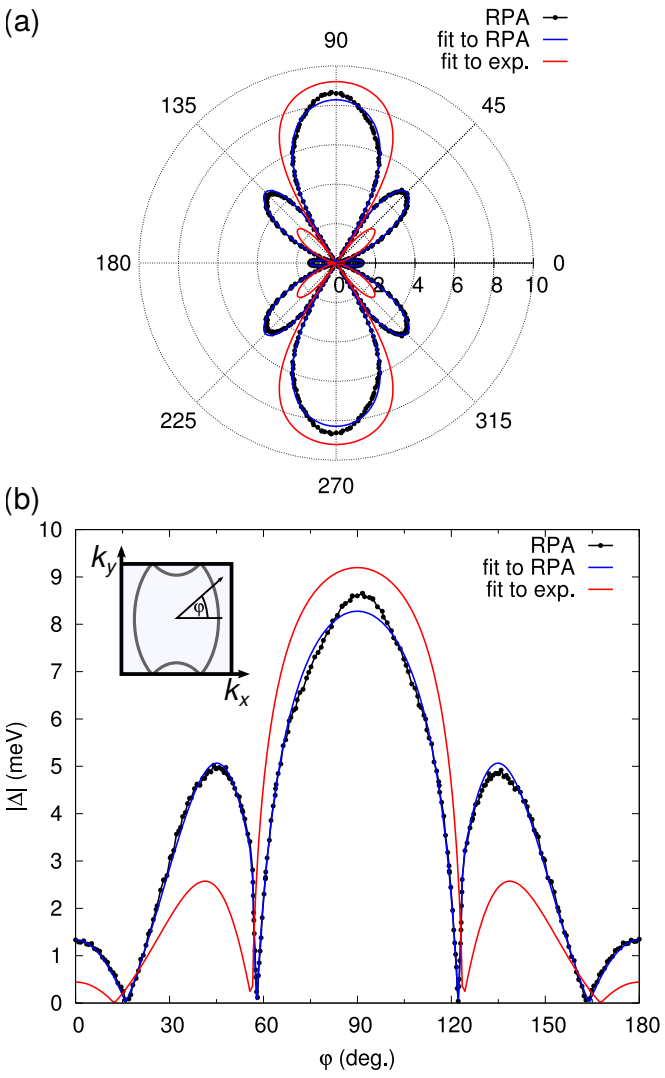

FIG. 11. (a) Polar and (b) linear plot of the magnitude of the superconducting gap $|\Delta|$ on the Fermi surface versus the angle φ measured from the k_x direction. For the RPA curves and the fit to experiment the energy scale was set to $\Delta_0 = 10$ meV and $\Delta_0 = 12.1$ meV respectively.

The static spin- and orbital-susceptibilities ($\chi^{s,\mathrm{RPA}}$ and $\chi^{c,\mathrm{RPA}}$) are constructed in an RPA framework. Since the interaction term in the Hamiltonian is local and our models are single-orbital in nature, we can restrict the calculation to the diagonal elements of the susceptibility and use scalar equations for the RPA-enhanced susceptibilities.

$$\chi_L^{s,\mathrm{RPA}}(\vec{q}) = \frac{\chi_L^0(\vec{q})}{1 - U\chi_L^0(\vec{q})},\ \chi_L^{c,\mathrm{RPA}}(\vec{q}) = \frac{\chi_L^0(\vec{q})}{1 + U\chi_L^0(\vec{q})}$$

Here, χ_L with $L = \{llll\}$ denotes the diagonal element of the susceptibility tensor associated with an BEDT-TTF site indexed by l. The total spin susceptibility is given by the sum over all site-resolved contributions $\chi^s(\vec{q}) = \frac{1}{2}\sum_L \chi_L^{s,\mathrm{RPA}}(\vec{q})$.

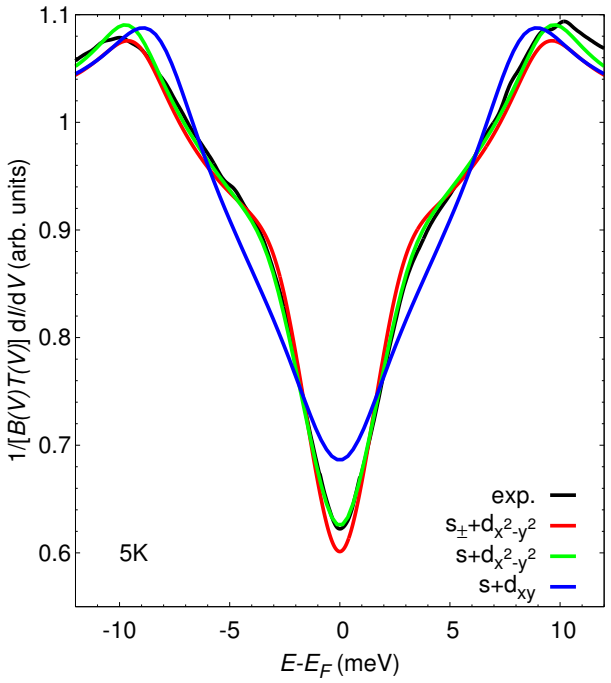

FIG. 12. Experimental spectrum at 5 K and simulation presented in the main paper ($s_\pm + d_{x^2-y^2}$) compared to simulated spectra of plain s-wave combined with d_{xy} and $d_{x^2-y^2}$ expressions.

The pairing vertex in orbital space for the singlet channel can be calculated using the fluctuation exchange approximation[19,20].

$$\Gamma_{spqt}(\vec{k},\vec{k}') = [\frac{1}{2}U\chi^{s,\mathrm{RPA}}(\vec{k}-\vec{k}')U + U\chi^{s,\mathrm{RPA}}(\vec{k}+\vec{k}')U - \frac{1}{2}U\chi^{c,\mathrm{RPA}}(\vec{k}-\vec{k}')U + U]_{spqt}$$

Momenta $\vec{k}$ and $\vec{k}'$ are restricted to the Fermi surface. As vectors $\vec{k} \pm \vec{k}'$ do not necessarily lie on the grid used in the calculation of the susceptibility $\chi^0(\vec{q})$, we use linear interpolation of the grid data.

The pairing vertex in orbital space is transformed into band space using the matrix elements $a_\mu^l(\vec{k})$.

$$\tilde{\Gamma}_{\mu\nu}(\vec{k},\vec{k}') = \mathrm{Re}\sum_{spqt} a_\mu^{t,*}(\vec{k})a_\mu^{p,*}(-\vec{k})[\Gamma_{spqt}(\vec{k},\vec{k}')] \times a_\nu^s(\vec{k}')a_\nu^q(-\vec{k}')$$

Finally, we solve the linearized gap equation by performing an eigendecomposition on the kernel and obtain the dimensionless pairing strength λ_i and the symmetry function $g_i(\vec{k})$.

$$-\sum_\nu \oint_{C_\nu} \frac{dk'_\parallel}{2\pi}\frac{1}{2\pi\, v_F(\vec{k}')}\left[\Gamma_{\mu\nu}(\vec{k},\vec{k}')\right] g_i(\vec{k}') = \lambda_i g_i(\vec{k})$$

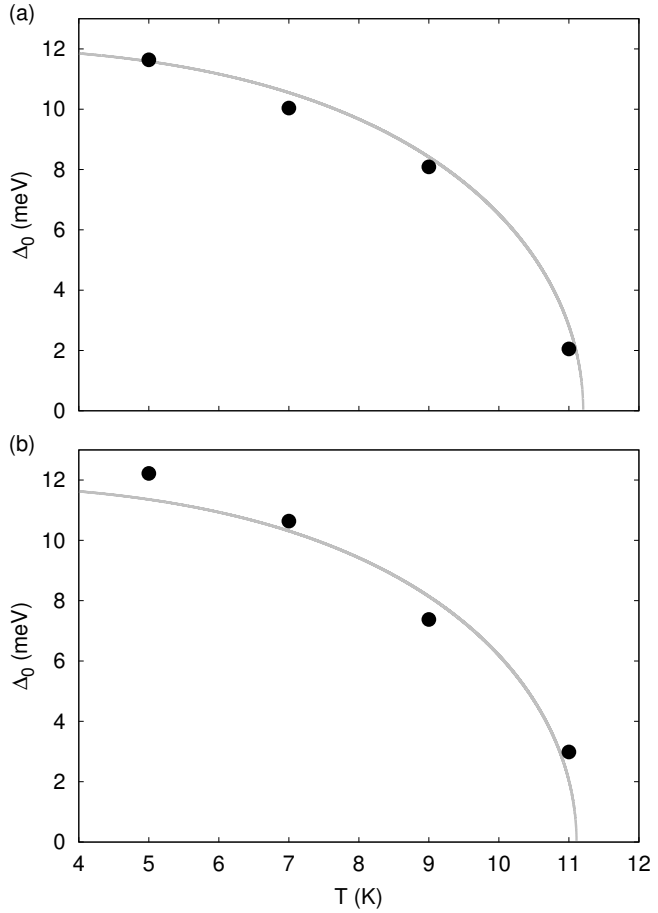

FIG. 13. Fit of the interpolation function for the solution of the s-wave BCS self consistency equation to the temperature dependent gap values obtained from the STS analysis. (a) shows the gaps extracted from the fit using prefactors c_i fixed to the values determined from the microscopic calculation, while (b) shows the gaps extracted from a fit to the STS experiment, where also the c_i were used as parameters.

In the gap equation we use the singlet symmetrized vertex $\Gamma_{\mu\nu}(\vec{k},\vec{k}') = \frac{1}{2}[\tilde{\Gamma}_{\mu\nu}(\vec{k},\vec{k}')+\tilde{\Gamma}_{\mu\nu}(\vec{k},-\vec{k}')]$. The integration runs over the discretized Fermi surface and $v_F(\vec{k})$ is the magnitude of the Fermi velocity.

XII. THEORY: RPA SPIN-FLUCTUATION PAIRING, COMPUTATIONAL DETAILS

For the intra-molecular Coulomb interaction we use a value of $U = 0.75$ eV. The non-interacting susceptibility is calculated on a 50×50 k-point grid at an inverse temperature of $\beta = 40$ eV^{-1}. For the solution of the gap equation we used 548 points on the two-dimensional Fermi surface.

* elmers@uni-mainz.de

[1] V. A. Ukraintsev, *Data evaluation technique for electron-tunneling spectroscopy*, Phys. Rev. B **53**, 11176 (1996).

[2] H. Shinaoka, and M. Imada, *Single-Particle Excitations under Coexisting Electron Correlation and Disorder: A Numerical Study of the Anderson-Hubbard Model*, J. Phys. Soc. Jpn. **78**, 094708 (2009).

[3] S. Diehl, T. Methfessel, U. Tutsch, J. Müller, M. Lang, M. Huth, M. Jourdan, and H.-J. Elmers, *Disorder-induced gap in the normal density of states of the organic superconductor κ-(BEDT-TTF)$_2$Cu[N(CN)$_2$]Br*, J. Phys.: Condens. Matter **27**, 265601 (2015).

[4] A. Savitzky and M. J. E. Golay, *Smoothing and Differentiation of Data by Simplified Least Squares Procedures*, Anal. Chem. **36**, 1627 (1964).

[5] O. J. Taylor, A. Carrington, and J. A. Schlueter, *Superconductor-insulator phase separation induced by rapid cooling of κ-(ET)$_2$Cu[N(CN)$_2$]Br*, Phys. Rev. B **77**, 060503(R) (2008).

[6] H. Padamsee, J. E. Neighbor, and C. A. Shiffman, *Quasiparticle phenomenology for thermodynamics of strong-coupling superconductors*, J. Low Temp. Phys. **12**, 387 (1973).

[7] O. J. Taylor, A. Carrington, and J. A. Schlueter, *Specific-Heat Measurements of the Gap Structure of the Organic Superconductors κ-(ET)$_2$Cu[N(CN)$_2$]Br and κ-(ET)$_2$Cu(NCS)$_2$*, Phys. Rev. Lett. **99**, 057001 (2007).

[8] K. Fujita, I. Grigorenko, J. Lee, J. X. Zhu, J. C. Davis, H. Eisaki, S. Uchida, and A. V. Balatsky, *Bogoliubov angle and visualisation of particle-hole mixtures in superconductors*, Phys. Rev. B **78**, 054510 (2008).

[9] P. E. Blöchl, O. Jepsen, and O. K. Andersen, *Improved tetrahedron method for Brillouin-zone integrations*, Phys. Rev. B **49**, 16223 (1994).

[10] R. C. Dynes, V. Narayanamurti, and J. P. Garno, *Direct Measurement of Quasiparticle-Lifetime Broadening in a Strong-Coupled Superconductor*, Phys. Rev. Lett. **41**, 1509 (1978).

[11] H. Elsinger, J. Wosnitza, S. Wanka, J. Hagel, D. Schweitzer, and W. Strunz, *κ-(BEDT-TTF)$_2$Cu[N(CN)$_2$]Br: A Fully Gapped Strong-Coupling Superconductor*, Phys. Rev. Lett. **84**, 6098 (2000).

[12] U. Geiser, A. J. Schultz, H. W. Wang, D. M. Watkins, D. L. Stupka, J. M. Williams, J. E. Schirber, D. L. Overmeyer, D. Jung, J. J. Novoa, and M.-H. Whangbo, *Strain index, lattice softness and superconductivity of organic donor-molecule salts, Crystal and electronic structures of three isostructural salts κ-(BEDT-TTF)$_2$Cu[N(CN)$_2$]X (X = Cl, Br, I)*, Physica C **174**, 475 (1990).

[13] D. Guterding, R. Valentí, H. O. Jeschke, *Influence of molecular conformations on the electronic structure of organic charge transfer salts*, Phys. Rev. B **92**, 081109(R) (2015).

[14] J. P. Perdew, K. Burke, and M. Ernzerhof, *Generalized Gradient Approximation Made Simple*, Phys. Rev. Lett. **77**, 3865 (1996).

[15] E. Yusuf, B. J. Powell, and R. H. McKenzie, *Antiferromagnetic spin fluctuations in the metallic phase of quasi-two-dimensional organic superconductors*, Phys. Rev. B **75**, 214515 (2007).

[16] S. Graser, T. A. Maier, P. J. Hirschfeld, and D. J. Scalapino, *Near-degeneracy of several pairing channels in multiorbital models for the Fe pnictides*, New J. Phys. **11**, 025016 (2009).

[17] D. Guterding, H. O. Jeschke, P. J. Hirschfeld, and R. Valentí, *Unified picture of the doping dependence of superconducting transition temperatures in alkali metal/ammonia intercalated FeSe*, Phys. Rev. B **91**, 041112(R) (2015).

[18] D. Guterding, S. Backes, H. O. Jeschke, and R. Valentí, *Origin of the superconducting state in the collapsed tetragonal phase of KFe_2As_2*, Phys. Rev. B **91**, 140503(R) (2015).

[19] N. E. Bickers, D. J. Scalapino, and S. R. White, *Conserving Approximations for Strongly Correlated Electron Systems: Bethe-Salpeter Equation and Dynamics for the Two-Dimensional Hubbard Model*, Phys. Rev. Lett. **62**, 961 (1989).

[20] D. J. Scalapino, E. Loh, Jr., and J. E. Hirsch, *d-wave pairing near a spin-density-wave instability*, Phys. Rev. B **34**, 8190 (1986).